Highlights

- H_2 dissociation on Co is promoted by undercoordinated sites
- But hydrogen atoms bind less strongly there compared to flat terrace sites
- In FTS steps and kinks may be the dominant source of surface hydrogen atoms

Graphical abstract

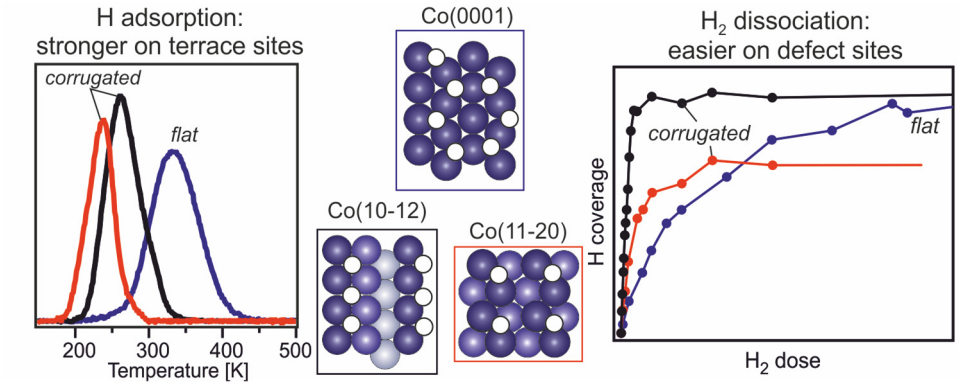

Interaction of hydrogen with flat (0001) and corrugated (11-20) and (10-12) cobalt surfaces: Insights from experiment and theory

C.J. (Kees-Jan) Weststrate[a], Mehdi Mahmoodinia[b], Mari Helene Farstad[b], Ingeborg-Helene Svenum[b,c], Marie D. Strømsheim[b], J.W. (Hans) Niemantsverdriet[a,d], Hilde J. Venvik[b]

[a]SynCat@DIFFER, Syngaschem BV, P.O. Box 6336, 5600 HH Eindhoven, The Netherlands

[b]Department of Chemical Engineering, Norwegian University of Science and Technology (NTNU), 7491, Trondheim, Norway

[c]SINTEF Industry, Postboks 4760 Torgarden, 7465 Trondheim, 7465, Norway

[d]SynCat@Beijing, Synfuels China Technology Co. Ltd., Leyuan South Street II, No. 1, Huairou District, 101407 Beijing, China

Abstract

Cobalt catalysts are used on a commercial scale to produce synthetic fuels via the Fischer-Tropsch synthesis reaction. Adsorbed hydrogen atoms are involved in many of the elementary reaction steps that occur on the catalyst surface. In this study we use a combination of experimental and theoretical methods to gain insight into how the structure of a cobalt surface affects the H_2 dissociation reaction and the adsorption bond strength of the hydrogen. A comparison of the open Co(11-20) and (10-12) surfaces with the flat, close packed Co(0001) surface shows that undercoordinated Co atoms strongly enhance the rate of H_2 dissociation. The lower desorption temperatures found on the more open surfaces indicate that the bond strength of adsorbed hydrogen decreases in the following order: Co(0001)>Co(10-12)>Co(11-20). DFT calculations confirm this trend, showing that hydrogen adsorbs weaker on the more open surfaces for both low and high coverages. In the context of the Fischer-Tropsch synthesis reaction we propose that step and kink sites are important for efficient H_2 dissociation. After dissociation, the higher hydrogen adsorption strength on terrace sites would promote diffusion away from the dissociation site to flat terraces where they can participate in hydrogenation reactions.

Introduction

In the Fischer-Tropsch synthesis reaction the carbon and oxygen atoms of the CO precursor molecule react with surface hydrogen atoms to form C_xH_y and H_2O. By using a cobalt-based catalyst operated at relatively low temperature, around or below 500 K, the selectivity of this reaction can be tuned to produce long chain aliphatic hydrocarbons. The product, synthetic wax of high purity, can be employed in various ways, one important route being the cracking of the syncrude to kerosene and diesel fractions to produce synthetic fuels of high purity.

The active phase of industrially applied cobalt catalysts consists of metallic nanoparticles with a typical size of around 5-10 nm [1]. One of the elementary reaction steps that occurs on the surface of these particles is the dissociative adsorption of H_2 to produce surface hydrogen atoms, the active species in hydrogenation steps on the surface.

Small metallic nanoparticles expose a heterogeneous surface with a large a variety of active sites. On fcc-cobalt particles flat (111) and (100) facets dominate, with monoatomic steps and kinks as the most common defect sites [2]. For metallic nanoparticles with a hcp bulk structure the close-packed (0001) surface can only be formed on two opposing sides of the particle, whereas the remaining sides expose more open surfaces [3,4] such as the (10-10) and the (10-11) surface. The Co(10-12) and Co(11-20) used in the present study are exposed as well on such particles.

Although the H_2 molecule is one of the reactants in FTS synthesis, there is only a limited number of studies in which the interaction of H_2 with single crystal surfaces of cobalt is discussed. On Co(0001) it has been found that the initial dissociative sticking coefficient of H_2 is not very high, with a value of around 0.01−0.05 [5–7]. The same studies show that the activation energy for desorption is in the order of 90-100 kJ mol^{-1}. After reaching a coverage

of 0.5 ML, the dissociative sticking coefficient decreases so much that UHV-type pressures are too low to produce a surface coverage beyond 0.5 ML [5–8].

Similar to other metal surfaces such as Pt and Ni [9], the surface atoms with a low coordination number which are exposed on step and kink sites have been shown to enhance H_2 dissociation on Co surfaces. On Co(0001) surface defects formed by a sputter treatment at room temperature enhance H_2 dissociation and a dissociative sticking coefficient close to unity is found on a defect-rich surface [5]. Surface defects furthermore allow the population of hydrogen sites associated with a dissociation barrier on the flat surface. In this way a coverage beyond 0.5 ML can be reached for a relatively low dose of H_2. Taking a somewhat different approach, Sykes and co-workers were able to prepare a (1×1) (1 ML) H_{ad} layer on Cu(111)-supported bilayer Co islands [10,11]. In this case the undercoordinated sites at the edges of the Co island facilitate H_2 dissociation. Beside these studies only the Co(10-10) surface has been studied experimentally [12]. Analysis of the thermal desorption spectra yielded an activation energy for desorption of 80 kJ mol^{-1}, significantly lower than that of the flat surface.

In the present study we use an experimental approach to study how the structure of the cobalt surface affects dissociative adsorption of the H_2 molecule. Our experiments also provide information about the adsorption strength of hydrogen atoms as a function of surface structure. The experimental work is complemented by an in-depth theoretical investigation in which we explore the adsorption site and adsorption strength of hydrogen atoms adsorbed on three different single crystal surfaces of cobalt. By systematically studying the effect of surface coverage we get insight into how lateral interactions affect the bond strength and determine which adsorption sites are the most preferred at each coverage.

Three different cobalt surfaces were used in this study: Co(0001), Co(10-12) and Co(11-20). The close-packed Co(0001) surface has been studied previously and serves as a reference point.

The other two surfaces were selected since they expose different types of undercoordinated surface atoms. In addition to this, their structure in the clean state is well-known, as earlier scanning tunnelling microscopy (STM) and low energy electron diffraction (LEED) studies have shown that their structure in the clean state is close to the bulk-terminated structure [13–15].

Materials and methods

Experimental procedures: The experiments were performed in a UHV system equipped with LEED/Auger optics, a sputter gun for sample cleaning and a differentially pumped quadrupole mass spectrometer. The disc-shaped samples were held in place by a U-shaped W support wire in thermal contact with a liquid nitrogen reservoir, allowing a temperature of around ~95 K. Sample heating was achieved by passing a direct current through the support wire. The sample temperature was measured by a K-type thermocouple, spotwelded to the backside of the sample. For both Co(0001) and Co(10-12) a disc-shaped single crystal with a thickness of 2 mm and a diameter of 8 mm was used. The Co(11-20) sample used in this study is disk-shaped, with a thickness of 1.5 mm thick and a diameter of 10 mm. The maximum temperature used in sample preparation and during experiments was kept below 670 K to stay clear from the hcp-fcc phase transition temperature of Co. Hydrogen doses are reported in Langmuir (1 L = 1×10^{-6} Torr·s) and were calculated using an ion gauge sensitivity factor of 0.35 to account for the low sensitivity for H_2.

A typical cleaning cycle consists of sputtering using 0.7-1 kV Ar^+ while the sample is held at 650-670 K, followed by annealing in vacuum at the same temperature. Sample cleanliness was checked by LEED and Auger. During the TPD experiment the sample was positioned 2 mm away from the 5 mm wide opening of the differentially pumped QMS housing to eliminate desorption from other parts of the sample holder from the desorption spectra. In this approach

the signal intensity depends on the exact distance between sample and the opening of the MS compartment, making a quantitative comparison of the amount of H_2 desorbed from two different samples complicated. The sample holder design minimizes the desorption from other parts of the sample holder, allowing us to use the pressure rise in the vacuum system during the TPD experiment for quantification. Since two samples can be mounted on the same sample holder it is possible to quickly change from one sample to another. By using the known saturation value of 0.5 ML on Co(0001) as a reference point [5–8] and taking the differences in surface area of the different samples into account we were able to determine the absolute quantity of H_2 desorbing from the (10-12) and (11-20) samples. Since the monolayer definition becomes ambiguous for the open surfaces used here we instead report hydrogen surface coverages as adsorbate atoms per nm^2.

Computational methods: All quantum chemical calculations reported here were carried out using spin-polarized DFT within the generalized gradient approximation (GGA). The projector-augmented wave (PAW) method [16,17] implemented in the Vienna Ab initio Simulation Package (VASP) [18,19] together with a plane wave basis set with 500 eV energy cut-off were used to describe the interactions between ion cores and valence electrons. The Perdew-Burke-Ernzerhof (PBE) functional [20,21] has been used for the exchange-correlation energy of electrons. The k-point sampling was performed with the Γ-centered Monkhorst-Pack scheme [22], and using a 5×5×1 k-point grid. The partial occupancies for each wavefunction were modelled by the approach proposed by Methfessel-Paxton [23] with a smearing width of 0.1 eV. The lattice parameters of bulk hcp Co were calculated as a=2.48 Å and c=4.04 Å. A magnetic moment of 1.64 μ_B per Co atom was obtained. These values are in good agreement with experimentally obtained values of a=2.51 and c=4.07 Å [24], and a magnetic moment of 1.72 μ_B/atom [25]. A five-layer slab with a vacuum region of about 10 Å between the repeating surfaces was used to model the Co(0001), Co(11–20) and Co(10–12) terminations, which were

represented using p(3×3), p(2×1), and p(3×1) surface unit cells, respectively. For structural relaxation calculations, the bottom two layers of atoms were kept fixed at their equilibrium positions, and the remaining layers were allowed to relax until the force components on each atom were less than 0.001 eV/Å.

The gas-phase H_2 molecule was calculated by placing it inside a simple cubic unit cell with 10 Å sides. The equilibrium bond distance of H_2 was calculated as 0.750 Å, in good agreement with the experimental value of 0.741 Å [26]. For the calculations of adsorbed hydrogen, the H atoms were adsorbed on one side of the Co surface slabs. To avoid artificial dipole effects, a dipole correction to the total energy was applied [27]. Vibrational frequency analyses were performed using the finite-difference method in order to identify the stationary points and also to include the zero-point vibrational correction to the adsorption energies. The zero-point energies (ZPE) of Co atoms were assumed to be unchanged upon adsorption, while the adsorbed H atoms were allowed to displace in each direction by ±0.015 Å. The adsorption energy (E_{ads}) of hydrogen atom on different adsorption sites of the corresponding surfaces were calculated as:

$$E_{ads} = (E_{slab+nH} + ZPE) - (E_{slab} + \frac{n}{2}(E_{H2} + ZPE))$$

where the E_{slab} , E_{slab+H}, and E_{H2} are total energies of the relaxed clean slabs, slabs with adsorbed H, and an isolated hydrogen molecule, respectively. Negative adsorption energy indicates that adsorption of H on the corresponding adsorption site is favourable. In order to study the effects of H coverage, and to probe the coverage-dependent differential adsorption energy curve, H atoms were sequentially introduced onto the Co surfaces, and the binding energy of the additional H atom was calculated as:

$$\Delta E_{ads} = E_{slab}^{(n+1)H} - E_{slab}^{nH} - \frac{1}{2} E_{H2}$$

were E_{slab}^{nH} and $E_{slab}^{(n+1)H}$ are ZPE-corrected total energies of slabs with n and $(n+1)H$ atoms, respectively. All possible high-symmetry adsorption sites were investigated for adsorption of H atoms and to study the effect of surface coverage. In order to facilitate comparison with experimental results, the H coverage is expressed as the number of H atoms per nm^2. All illustrations of the optimized geometries were produced using the Visualization for Electronic and Structural Analysis (VESTA) program [28].

Experimental Results

Fig. 1 shows the structure of the three Co surfaces investigated. The LEED patterns of the clean surface indicate a good surface quality of the samples. It should be noted that two possible terminations exist for the Co(10-12) plane. Previous studies concluded that the A-termination is preferred [15], and this structure is investigated here.

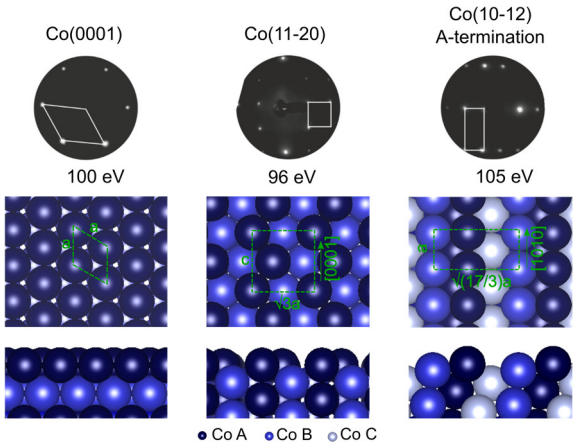

Fig. 1: Surface structure (top and side views) and LEED patterns of the Co(0001), Co(11–20), and the Co(10–12) surfaces. The surface unit cells and lattice parameters are indicated. For the corrugated surfaces the labels A, B and C are used to indicate the layer in which the cobalt atom is located.

Hydrogen adsorption and desorption: Temperature programmed desorption was used to study the adsorption and desorption dynamics of H_2. Fig. 2 shows a series of H_2 desorption

spectra after dosing the indicated quantity of H_2 to the three different samples held at 100 K during exposure to H_2.

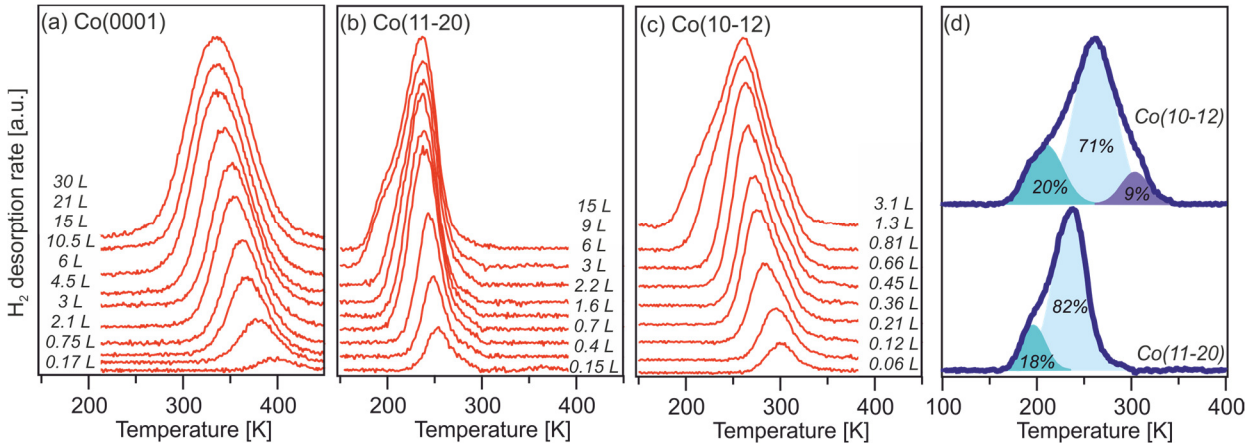

Fig. 2: H_2 desorption spectra after dosing H_2 at a sample temperature of 100 K on the three different surfaces. A heating rate of 2 Ks^{-1} was used in all cases.

In line with previous reports [5–7], the H_2 desorption spectra for the flat surface, shown in Fig. 2(a), consist of a single H_2 desorption peak. The downward shift of the peak maximum with increasing hydrogen coverage, from 400 K for the lowest coverage to 330 K for the highest coverage, is typical for a second order desorption process such as expected for the recombinative desorption of two H_{ad} to form H_2. The previously established H_{ad} saturation coverage of 0.5 ML (9.15 H per nm^2) is reached after a dose of ~30 L.

Desorption from the more open Co(11-20) surface, shown in Fig. 2(b), occurs at a much lower temperature. The desorption peak maximum shows a modest shift as a function of surface coverage, from 254 K for low coverage to 235 K for high coverage. This high temperature desorption peak saturates after dosing 6 L, whereas a small shoulder develops for higher exposures which reaches a saturation point after a dose of 9 L. As described in the experimental section, the system pressure rise caused by desorption of 0.5 ML H_{ad} from the Co(0001) sample was used as a reference to quantify the hydrogen coverage on the Co(11-20) surface. This

approach yields a hydrogen coverage of 6.8 hydrogen atoms per nm^2 for the highest coverage observed in our experiment. Deconvolution of the spectrum using two peaks with a gaussian shape, shown in Fig. 2(d), reveals that the main peak, centred at 240 K, accounts for ~5.6 hydrogens per nm^2, whereas the shoulder centred at 195 K accounts for ~1.2 hydrogens per nm^2. Since the density of row atoms is 11.3 per nm^2 on Co(11-20), this implies that the 240 K desorption peak corresponds to 1 H_{ad} per two zigzag row atoms.

For the Co(10-12) surface the desorption of hydrogen occurs between 200-320 K. A small high temperature desorption peak centred around 300 K saturates after a small dose of 0.12 L already. The main desorption peak saturates after a dose of around 1 L, with the peak maximum at the saturation point located at 260 K. A low temperature shoulder develops for exposures >1 L, reaching a saturation point around 3 L (spectra for higher doses not shown here). Quantitative analysis shows a coverage of 9.3 hydrogen atoms per nm^2 at this point, that is, 1.4 hydrogen atoms per surface unit cell [see Fig. 1(c)]. Fig. 2(d) shows that the spectrum after dosing 3 L can be deconvoluted into three components, where the high temperature shoulder accounts for ~9% of the total. The main peak accounts for 71% of the total whereas the low temperature shoulder accounts for 20% of the total. Thus, after saturation of the main desorption peak centred at 260 K, the surface hydrogen concentration equals ~1 H_{ad} per surface unit cell.

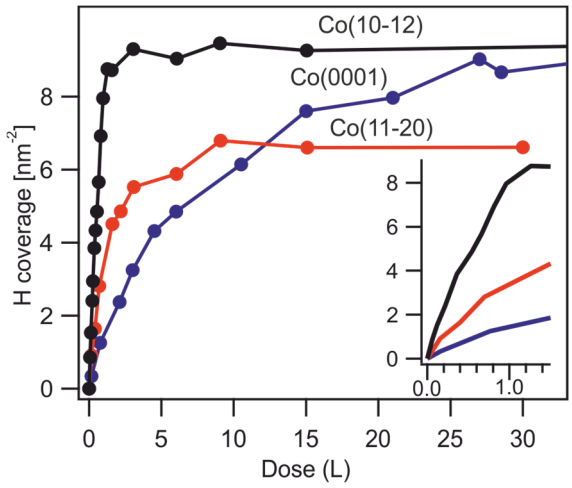

Fig. 3: Hydrogen coverage as a function of dose for the three different Co surfaces held at 100 K.

Fig. 3 shows the hydrogen coverage as a function of H_2 dose for the three surfaces investigated in this work. This graph clearly illustrates that the dissociative sticking coefficient of H_2 strongly depends on the structure of the surface. The Co(10-12) surface is the most reactive, requiring only a dose of ~1 L to reach saturation. Although the Co(11-20) surface also exposes a large concentration of surface atoms with a low coordination number, the initial sticking coefficient for H_2 on this surface is ~32% of that of the Co(10-12) surface. The initial sticking coefficient is lowest on the Co (0001), around only 10% of the value for the Co(10-12) surface.

Computational Results

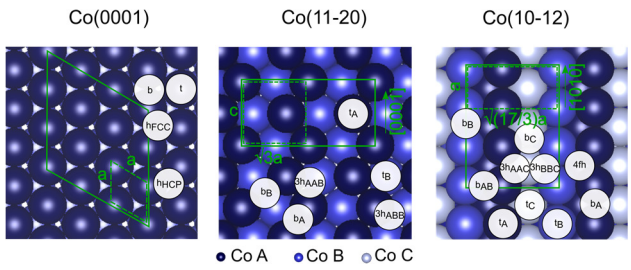

Fig. 4: Top views of the Co(0001), Co(11–20), and the Co(10–12) surface models together with the adsorption sites considered for each surface slab. The unit cell of each surface, and the surface unit cells used for the calculations, are indicated with dotted and solid green lines, respectively. The letters t, b and h stand for top, bridge and hollow adsorption sites.

DFT calculations were performed to further investigate how the adsorption strength of hydrogen depends on the structure of the cobalt surface. Fig. 4 illustrates the surface unit cells of the model Co surfaces used for the DFT calculations, where the different high symmetry sites explored for hydrogen adsorption are labelled. The Co(0001) surface exhibits four different sites: i.e. top (t), bridge (b), fcc-hollow (h_{FCC}), and hcp-hollow (h_{HCP}) sites [Fig. 4(a)]. The Co(11–20) facet exposes a corrugated surface with zigzag rows of Co atoms along the [0001] direction [Fig. 1(b)]. The atoms in the outermost rows have a coordination number of 7 and are referred to as the A-layer. The surface atoms between the rows have a coordination number of 11 and are referred to as the B-layer. This surface contains a larger number of high symmetry sites, namely two types of top sites, (t_A, t_B), two types of bridge sites (b_A, b_B), and two different types of 3-fold-hollow ($3h_{AAB}$, $3h_{ABB}$) sites, as indicated in Fig. 4(b). The Co(10–12) surface consist of three different layers and exhibits an even larger number of possible adsorption sites, namely; three top sites, (t_A, t_B, t_C), four bridge sites, (b_A, b_B, b_C, b_{AB}), two 3-fold hollow ($3h_{AAC}$, $3h_{BBC}$) sites, and one 4-fold hollow (4fH) sites, as indicated in Fig. 4(c). It exposes atoms in two layers below the top rows and may be regarded as a stepped surface.

H adsorption at low coverages: The energetic and structural parameters for adsorption of a single hydrogen atom per unit cell on various high symmetry adsorption sites of the p(3×3), p(2×1), and p(3×1) surface unit cells of the Co(0001), Co(11–20), and Co(10–12) surfaces, respectively, are listed in Table 1. It is worth mentioning that the calculated adsorption energies for "unstable" sites are obtained by fixing the position of the H atom along the x- and y-axes, i.e., in the surface plane, and relaxing the distance along the z-axis. Otherwise, a complete relaxation of geometry results in moving the H atoms to nearby stable sites.

For the close-packed (0001) surface, the most favourable adsorption site for a single H atom in the p(3×3) unit cell is the h_{FCC} site, followed by a h_{HCP} site (Fig. 4), with the adsorption energies of –0.50 eV, and –0.47 eV, respectively (Table 1). This is in good agreement with a previous

DFT study on the Co(0001) and Co(111) surfaces [29]. The presence of imaginary modes in the calculation of the vibrational modes show that bridge (B) and top (T) sites are not the local minima, and the energy values were obtained by fixing the x and y coordinate as discussed in the previous paragraph.

For the Co(11–20) facet, H adsorbs preferentially in the $3h_{AAB}$ site, where H binds to two A-row and one B-row atoms of the Co surface. The adsorption energy is –0.34 eV, only slightly larger than the H in the b_A site (–0.32 eV). This is, however, considerably lower compared to the adsorption energy found for H on the Co(0001) surface. Hence, this can explain the low H_2 desorption temperature of around 250 K obtained experimentally for this surface in comparison to 400 K for Co(0001).

For the Co(10–12) surface the calculations show that the 4fH site is the most favourable adsorption site, with an adsorption energy of –0.47 eV, almost the same as the most favourable site on the Co(0001) surface. The bridge site between two atoms in the B layer, (b_B), is the second-most favourable site followed by $3h_{AAC}$, and $3h_{BBC}$ sites, respectively. Hydrogen adsorption was not stable at the top and b_A sites, and the adsorbate moved to nearby stable sites during relaxation. This is corroborated with the presence of imaginary modes in the calculated vibrational modes presented in Table 1. The decreasing adsorption energy from Co(0001) to Co(10-12) to Co(11-20) is qualitatively in line with the trend in the desorption temperatures observed in the low coverage TPD spectra (Fig. 2) for the three surfaces.

Table 1: Zero-point energy corrected adsorption energies (E_{ads}), the nearest distance to the Co atoms (d_{Co-H}), and lists of the calculated vibrational frequencies (ν_i) of a hydrogen atom adsorbed at the various adsorption sites on the Co surfaces. Adsorption sites are illustrated in Fig. 4.

Facet/Slab	site	E_{ads}(eV)	d_{Co-H}(Å)	$\nu_i [cm]^{-1}$
(0001)	t	0.06	1.51	1796, 369i, 369i
p(3×3)	b	–0.37	1.67	1260, 1123, 496i
	h_{HCP}	–0.47	1.74	1123, 823, 823
	h_{FCC}	**–0.50**	**1.73**	**1133, 877, 877**
(11-20)	t_A	0.13	1.53	1782, 125i, 382i
p(2×1)	t_B	–0.21	1.63	1371, 329i, 437i
	b_A	–0.32	1.67	1344, 1055, 285
	b_B	–0.28	1.79	980, 843, 624
	$3h_{AAB}$	**–0.34**	**1.72**	**1147, 783, 495**
	$3h_{ABB}$	–0.26	1.76	983, 875, 611
(10-12)	t_A	0.06	1.53	1739, 315i, 439
p(3×1)	t_B	0.03	1.52	1794, 110i, 384i
	t_C	–0.31	1.63	1357, 198, 425i
	b_A	–0.29	1.66	1253, 1073, 163i
	b_B	–0.38	1.66	1294, 1138, 260
	b_C	–0.32	1.77	960, 949, 652
	b_{AB}	–0.31	1.65	1319, 1048, 93
	$3h_{AAC}$	–0.36	1.72	1109, 888, 771
	$3h_{BBC}$	–0.35	1.75	1107, 898, 641
	4fH	**–0.47**	**1.89**	**791, 621, 561**

Coverage effect on H adsorption: The influence of coverage on the hydrogen adsorption strength was systematically investigated by adding hydrogen atoms to the unit cell and exploring various possible configurations to determine the one with the lowest total energy. Figs. 5(a)-(f) show two different coverages for the three surfaces to illustrate the occupation of different adsorption sites with increasing coverage. The differential adsorption energy is commonly used to follow the build-up towards the saturation coverage on surfaces [30], as it gives the amount of energy gained by adding a new adsorbate to the existing coverage. Figs. 5(g) shows the calculated differential adsorption energies as a function of H coverage per nm^2 for all three Co surfaces. The saturation coverage is given by the point where the differential adsorption energy becomes positive.

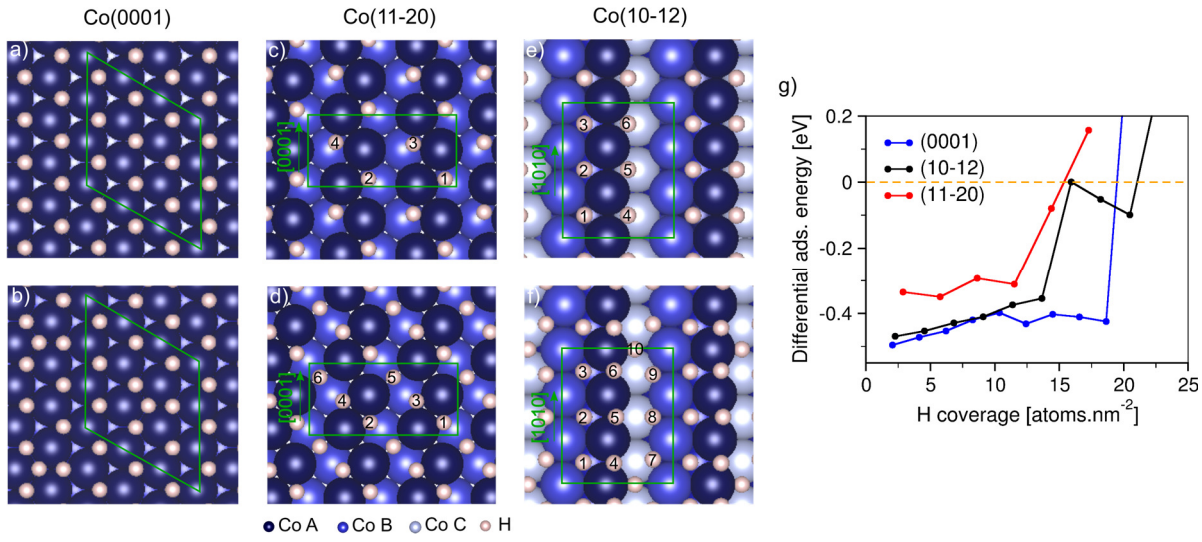

Fig. 5: Hydrogen adsorption sites and energies as a function of coverage. (a-f) show the hydrogen adsorption sites for two different coverages for Co(0001), Co(11-20) and Co(10-12), with (c-f) showing the order in which the surface sites are filled following the lowest energy pathway. (g) shows the differential adsorption energies of H atoms as a function of coverage for Co(0001), Co(10–12), and Co(11–20).

For Co(0001), the strongest adsorption site is the 3-fold FCC hollow (h_{FCC}) site, and these sites are occupied exclusively during the process of covering the surface with hydrogen. It is worth

mentioning that combinations of FCC and HCP hollow site occupation were also considered for a different H coverage. However, in all cases occupation of the FCC sites was found to be energetically most favourable. The differential adsorption energy slightly decreases (becomes less negative) with increasing coverage, indicating that lateral interactions reduce the adsorption energy of hydrogen. The adsorption energy increases sharply when additional hydrogen is added after all h_{FCC} sites are filled. Fig. 5(a) shows a model of the adsorbate-covered surface at this point. When more hydrogen is added the h_{HCP} sites start to be populated, as shown in Fig. 5(b). This is energetically unfavourable, and the differential adsorption energy becomes positive at this point. Since the energy differences between different configurations at a given coverage on Co(0001) were negligible we did not include the order in which the sites are filled in Fig. 5(a,b).

For the Co(11-20) surface we find that the second hydrogen added to the (2×1) unit cell preferentially occupies a $3h_{AAB}$ site located in a different row on the surface. The third and fourth hydrogen atoms adsorb with a slightly lower differential adsorption energy and occupy the next $3h_{AAB}$ sites along the A-row Co atoms indicated as 3 and 4 in Fig. 5(c). However, these H-atoms shift to the adjacent $3h_{AAB}$ sites (indicated as 3 and 4 in Fig. 5(d)) upon addition of the hydrogen atoms occupying positions 5 and 6. This is due to the repulsive interactions caused by close proximity of H atoms in 3 and 4 to the newly adsorbed H in positions 5 and 6. Consequently, the added hydrogen not only adsorbs less strongly, but it also destabilizes the hydrogen atoms that are already present. This combined effect explains why adding a fifth hydrogen causes a step change in the differential adsorption energy, and a similarly large step change following the addition of a sixth hydrogen in the unit cell shifts the differential adsorption energy above zero [Fig. 5(g)].

For the Co(10–12), the most favourable adsorption site is the 4-fold hollow site, and up to three H atoms are accommodated on these sites in the (3×1) unit cell, as shown in Fig. 5(e). Although

the bridge site between two atoms in the B-layer, b_B, is the second-most stable adsorption site for low coverage, we find that adsorption in these sites is disfavoured when the adjacent 4-fold hollow sites are filled. Instead, the 3-fold-hollow sites ($3h_{BBC}$) indicated as 4, 5, and 6 in Fig. 5(e) are occupied. When additional hydrogen atoms are added they occupy the 7, 8, and 9 positions on the surface. Filling of these sites leads to a destabilization of the hydrogens adsorbed in positions 4,5 and 6, and as a consequence they slightly move toward the b_B sites, as shown in Fig. 5(f). At this point the coverage is already rather high, and the differential adsorption energy plot [Fig. 5(g)] shows an overall decrease in stability due to increasing coverage from 6H to 9H per (3×1) unit cell (from 13.4 to 20.1 H per nm^2). This may be attributed to lateral interactions between the hydrogen adsorbates. However, increasing the H coverage beyond 9 H (20.1 H per nm^2) is no longer energetically favourable as evident from the positive differential adsorption energy.

Discussion

Since adsorbed hydrogen atoms are directly involved in the elementary reaction steps that affect the activity and the selectivity of the FTS reaction [31] it is worthwhile to explore the structure dependence of hydrogen adsorption in detail. The experimental data shown here indicate that the influence of surface structure on the adsorption of hydrogen is surprisingly large, and both the adsorption kinetics, that is, the dissociative sticking probability, as well as the adsorption strength of adsorbed hydrogen atoms depend on the structure of the surface.

Hydrogen adsorption strength and H_2 desorption temperature

The TPD data shows that the hydrogen desorption temperature is a strong function of coverage. This is in agreement with the DFT calculations, which show that the hydrogen adsorption strength is the highest for hydrogen adsorbed in the 3-fold hollow sites on Co(0001). By using a second-order Redhead method [32] with an assumed pre-exponential factor of 1×10^{13} ML^{-1}

s^{-1} we find an activation energy for H_2 desorption of 92 (±7) kJ mol^{-1} (0.48 ± 0.04 eV/H_{ad}) in the low coverage regime (θ_H = 0.07 ML), close to the computed value and in line with earlier work [5]. On Co(10-12), H_{ad} instead prefers to adsorb in the 4-fold hollow site, but its bond strength is lower than that on the close-packed surface. A simple Redhead analysis of the main desorption peak yields a barrier of ~72(±5) kJ mol^{-1} (0.37 ± 0.03 eV/H_{ad}), somewhat lower than the computed adsorption energy of hydrogen on this surface. Hydrogen adsorbs weakest on the Co(11-20) surface. Although threefold hollow sites are available on this surface, the low H_2 desorption temperature, around 250 K, shows that the hydrogen adsorbs much weaker in these sites compared to the threefold sites on the Co(0001) surface. This is confirmed by the DFT calculations, which show a particularly low differential heat of adsorption on the Co(11-20) surface. In this case the Redhead approach for second order desorption yields a desorption barrier of around 61(±4) kJ mol^{-1} (0.316 ±0.02 eV/H_{ad}) for the main desorption peak, close to the value found in our computational study.

Hydrogen saturation coverage and the role of defect sites

The theory calculations shown in Fig. 5 indicate that it is energetically feasible to adsorb up to 1 ML of hydrogen on the Co(0001) surface. This coverage cannot be reached on a single crystal surface with low defect density, since the dissociative sticking coefficient drops to a very low value for θ_H>0.5 ML. In other words, the experimentally observed H_{ad} saturation coverage of 0.5 ML H_{ad} is kinetically limited. For the close-packed surfaces the effect of defects is twofold: (i) the initial sticking coefficient for dissociative H_2 adsorption increases by one or two orders of magnitude, and (ii) the sticking coefficient for θ_H>0.5 ML remains high so that the saturation coverage of ~1 ML can be reached [5,11].

Our findings confirm that H_2 dissociation is much easier on the open Co surfaces in comparison to the close-packed surface. But despite the high *initial* dissociative sticking coefficient of H_2

dissociation the saturation coverage reached in the experiment is low: for the Co(11-20), which exposes zig-zag rows of 7-coordinated atoms, the peak that corresponds to the desorption of the most strongly bound hydrogens is equal to 1 H_{ad} per two row atoms. Although it is possible to adsorb more hydrogen onto this surface, it adsorbs even less strongly.

The Co(10-12) surface exposes a number of different adsorption sites for hydrogen. Apart from the fourfold hollow site two different kinds of threefold site can be identified. For this surface the desorption peak attributed to the most strongly bound hydrogen saturates at around one H_{ad} per unit cell, assigned to complete occupation of the 4-fold hollow site as indicated by the DFT calculations. A small amount of additional hydrogen can be accommodated on the 3-fold sites, but at a lower adsorption energy.

For both surfaces, the experimentally observed saturation coverage is around two times lower than the maximum coverage that is feasible according to the DFT calculations. This implies that kinetic limitations are at play in limiting the experimentally observed saturation coverage. We explain this by a self-poisoning effect of the active sites for H_2 dissociation. Both the Co(11-20) and Co(10-12) surface expose undercoordinated sites that readily dissociate the H_2 molecule. However, on these open surfaces the active sites for H_2 dissociation are also the most favourable for H_{ad} to reside. This makes the diffusion of the H-atoms away from the active site for dissociation unfavourable and will eventually lead to strong suppression of H_2 dissociation. This is different on defective Co(0001). In this case the defects are the most active for H_2 dissociation, but the dissociation product, H_{ad}, is most strongly bound in threefold hollow sites on extended terrace sites. This provides a driving force for diffusion of H_{ad} away from the active site for H_2 dissociation. In this way poisoning of the active site for H_2 dissociation is circumvented, and a θ_H of around 1 ML can be reached on defect-rich Co(0001).

Relevance for Fischer-Tropsch synthesis

Adsorbed hydrogen atoms are involved in many of the elementary reaction steps in Fischer-Tropsch synthesis. The present work highlights that dissociative adsorption of H_2 is a reaction step for which the rate depends strongly on the structure of the catalyst surface. In addition to this, the adsorption strength of surface hydrogen is different on different surface facets and varies with hydrogen coverage. A prominent finding in our study concerns the role that undercoordinated surface atoms play. On the one hand, they efficiently catalyse the H-H bond breaking, but on the other hand, the dissociation product, hydrogen atoms, bind less strongly to those undercoordinated sites than they do to the preferred symmetric 3-fold hollow sites. The cobalt nanoparticles in a Co-based cobalt catalyst typically adopt the fcc bulk structure, where the particle surface is dominated by (111) and (100) terraces terminated by step sites [2]. The findings here indicate that H_2 dissociation is much more efficient on step sites than on flat terrace sites. Our work indicates stronger adsorption of these hydrogen atoms on the terrace sites, so spill-over from the step sites to the terrace sites is feasible.

In this context, it is interesting to discuss the particle size effect that has been reported for cobalt catalysts. A SSITKA study reported by den Breejen et al. [33] indicated that the surface hydrogen concentration increases when particles become small. This can be rationalized by the findings presented here. Smaller particles expose more steps and kink sites, making it easier for the hydrogen to dissociate.

Conclusions

The present study shows that the interaction of H_2 with cobalt surfaces strongly depends on the exact structure of the surface. By combining experiments with theory-based calculations, we show that the dissociative adsorption of H_2 is strongly enhanced by undercoordinated surface atoms. Furthermore, we find that H_{ad} is most strongly adsorbed in 3-fold hollow sites such as

exposed by the close-packed hexagonal surface, whereas adsorption on the more open surfaces is significantly weaker.

Literature

[1] J. van de Loosdrecht, F.G. Botes, I.M. Ciobica, A. Ferreira, P. Gibson, D.J. Moodley, A.M. Saib, J.L. Visagie, C.J. Weststrate, J.W. Niemantsverdriet, in: J. Reedijk, K. Poeppelmeier (Eds.), Compr. Inorg. Chem. II, 2nd ed., Elsevier Ltd., 2013, pp. 525–557.

[2] P. van Helden, I.M. Ciobîcă, R.L.J. Coetzer, Catal. Today 261 (2016) 48–59.

[3] J.X. Liu, H.Y. Su, D.P. Sun, B.Y. Zhang, W.X. Li, J. Am. Chem. Soc. 135 (2013) 16284–16287.

[4] Q. Chen, I.-H. Svenum, Y. Qi, L. Gavrilovic, D. Chen, A. Holmen, E.A. Blekkan, Phys. Chem. Chem. Phys. 19 (2017) 12246–12254.

[5] P. van Helden, J.-A. van den Berg, C.J. Weststrate, ACS Catal. 2 (2012) 1097–1107.

[6] K.M.E. Habermehl-Ćwirzeń, K. Kauraala, J. Lahtinen, Phys. Scr. T108 (2004) 28–32.

[7] Z. Huesges, K. Christmann, Zeitschrift Fur Phys. Chemie 227 (2013) 881–899.

[8] D. Klinke, L. Broadbelt, Surf. Sci. 429 (1999) 169–177.

[9] K. Christmann, Surf. Sci. Rep. 9 (1988) 1–163.

[10] E.A. Lewis, D. Le, A.D. Jewell, C.J. Murphy, T.S. Rahman, E.C.H. Sykes, ACS Nano 7 (2013) 4384–4392.

[11] E.A. Lewis, M.D. Marcinkowski, C.J. Murphy, M.L. Liriano, E.C.H. Sykes, J. Phys. Chem. Lett. 5 (2014) 3380–3385.

[12] K.-H. Ernst, E. Schwarz, K. Christmann, J. Chem. Phys. 101 (1994) 5388.

[13] H.J. Venvik, C. Berg, A. Borg, Surf. Sci. 402–404 (1998) 57–61.

[14] M.D. Strømsheim, I.H. Svenum, M.H. Farstad, Z. Li, L. Gavrilovic, X. Guo, S. Lervold, A. Borg, H.J. Venvik, Catal. Today 299 (2018) 37–46.

[15] K.A. Prior, K. Schwaha, M.E. Bridge, R.M. Lambert, Chem. Phys. Lett. 65 (1979) 472–475.

[16] P.E. Blöchl, Phys. Rev. B 50 (1994) 17953–17979.

[17] G. Kresse, D. Joubert, Phys. Rev. B - Condens. Matter Mater. Phys. 59 (1999) 1758–1775.

[18] G. Kresse, J. Furthmüller, Comput. Mater. Sci. 6 (1996) 15–50.

[19] G. Kresse, J. Furthmüller, Phys. Rev. B - Condens. Matter Mater. Phys. 54 (1996) 11169–11186.

[20] J.P. Perdew, K. Burke, M. Ernzerhof, Phys. Rev. Lett. 77 (1996) 3865–3868.

[21] J.P. Perdew, K. Burke, M. Ernzerhof, Phys. Rev. Lett. 77 (1996) 3865–3868.

[22] H.J. Monkhorst, J.D. Pack, Phys. Rev. B 13 (1976) 5188–5192.

[23] M. Methfessel, A.T. Paxton, Phys. Rev. B 40 (1989) 3616–3621.

[24] A. Taylor, R.W. Floyd, Acta Crystallogr. 3 (1950) 285–289.

[25] D.R. Lide, H. V. Kehiaian, Handbook of Thermophysical and Thermochemical Data, 1st ed., CRC Press, Boca Raton, FL, 1994.

[26] K.P. Huber, G. Herzberg, Molecular Spectra and Molecular Structure 4: Constants of Diatomic Molecules, Van Norstrand Reinhold. Co., New York, USA, 1979.

[27] L. Bengtsson, Phys. Rev. B - Condens. Matter Mater. Phys. 59 (1999) 12301–12304.

[28] K. Momma, F. Izumi, J. Appl. Crystallogr. 44 (2011) 1272–1276.

[29] N. Atodiresei, V. Caciuc, P. Lazić, S. Blügel, Phys. Rev. Lett. 102 (2009) 1–4.

[30] S. Gudmundsdóttir, E. Skúlason, K.-J. Weststrate, L. Juurlink, H. Jónsson, Phys. Chem. Chem. Phys. 15 (2013) 6323–32.

[31] C.J. Weststrate, J.W. Niemantsverdriet, Faraday Discuss. 197 (2016) 101–116.

[32] P.A. Redhead, Vacuum 12 (1962) 203–211.

[33] J.P. Den Breejen, P.B. Radstake, G.L. Bezemer, J.H. Bitter, V. Frøseth, A. Holmen, K.P. de Jong, J. Am. Chem. Soc. 131 (2009) 7197–7203.